HHS Public Access

Author manuscript

ACS Nano. Author manuscript; available in PMC 2019 November 28.

Published in final edited form as:

ACS Nano. 2019 November 26; 13(11): 12345–12356. doi:10.1021/acsnano.9b03912.

Self-Activated Electrical Stimulation for Effective Hair Regeneration *via* a Wearable Omnidirectional Pulse Generator

Guang Yao[†,§,#], **Dawei Jiang**[‡,∥,#], **Jun Li**[†], **Lei Kang**[‡], **Sihong Chen**[§], **Yin Long**[†,§], **Yizhan Wang**[†], **Peng Huang**[∥], **Yuan Lin**[§], **Weibo Cai**[*,‡], **Xudong Wang**[*,†]

[†]Department of Materials Science and Engineering, University of Wisconsin—Madison, Madison, Wisconsin 53706, United States

[‡]Department of Radiology, University of Wisconsin—Madison, Madison, Wisconsin 53705, United States

[§]State Key Laboratory of Electronic Thin Films and Integrated Devices, University of Electronic Science and Technology of China, Chengdu, Sichuan 610054, P.R. China

[∥]Guangdong Key Laboratory for Biomedical Measurements and Ultrasound Imaging, Carson International Cancer Center, Laboratory of Evolutionary Theranostics, School of Biomedical Engineering, Health Science Center, Shenzhen University, Shenzhen 518060, China

Abstract

Hair loss, a common and distressing symptom, has been plaguing humans. Various pharmacological and nonpharmacological treatments have been widely studied to achieve the desired effect for hair regeneration. As a nonpharmacological physical approach, physiologically appropriate alternating electric field plays a key role in the field of regenerative tissue engineering. Here, a universal motion-activated and wearable electric stimulation device that can effectively promote hair regeneration *via* random body motions was designed. Significantly facilitated hair regeneration results were obtained from Sprague–Dawley rats and nude mice. Higher hair follicle density and longer hair shaft length were observed on Sprague–Dawley rats when the device was employed compared to conventional pharmacological treatments. The device can also improve the

[*]**Corresponding Authors:** wcai4@wisc.edu. xudong.wang@wisc.edu.

[#]G.Y. and D.J. contributed equally to this work.

Author Contributions

X.W. and G.Y. conceived the concept. X.W. and W.C. provided lab assistance. X.W., W.C., Y.L., and P.H. supervised the project. G.Y. and J.L. fabricated devices and tested the strain–stress curves and voltage signals. G.Y., S.C., and Y. L. made electric field and mechanical simulations. Y.W. took the pictures of scanning electron microscope. D.J. and G.Y. performed the experiments of SD rats and nude mice with different hair regeneration times. G.Y. and L.K. performed the experiments of SD rats based on electrodes of different shapes. X.W., G.Y., D.J., and W.C. analyzed the data and wrote the manuscript. All authors reviewed and commented on the manuscript.

Supporting Information

The Supporting Information is available free of charge on the ACS Publications website at DOI: 10.1021/acsnano.9b03912. Detailed fabrication process of the *m*-ESD; performance characterization of the Ecoflex band and PTFE film; computational and experimental mechanical properties of the *m*-ESD; mechanical compliance and robustness of the *m*-ESD; biocompatible performance of the *m*-ESD; four different configurations of CTE and corresponding CGE; images of the rat treated with sham *m*-ESD and *m*-ESD with interdigitated and W-shaped electrodes, respectively; hair regeneration under different stimulation methods; H&E staining of horizontal slices in different regions for SD rats; *m*-ESD for nude mice; images of hair under the influence of *m*-ESD, MNX, VD_3, and NS with a hand-held digital microscope; optical images of nude mice without treatment; H&E staining of longitudinal slices of the epidermis under different stimulation time for nude mice; H&E staining of horizontal slices over time for nude mice (PDF)

The authors declare no competing financial interest.

secretion of vascular endothelial growth factor and keratinocyte growth factor and thereby alleviate hair keratin disorder, increase the number of hair follicles, and promote hair regeneration on genetically defective nude mice. This work provides an effective hair regeneration strategy in the context of a nonpharmacological self-powered wearable electronic device.

Graphical Abstract

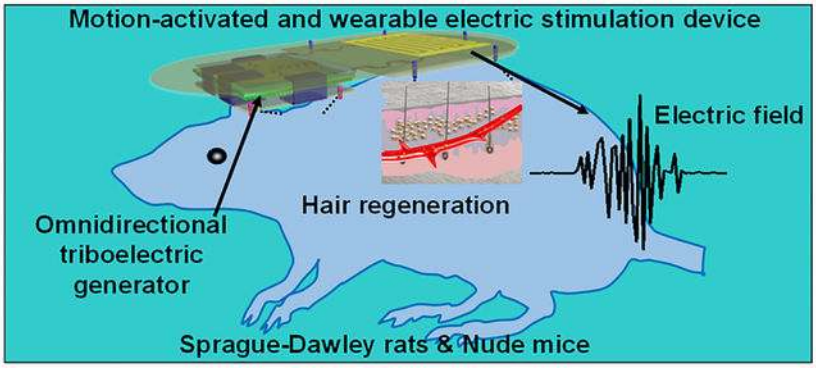

Keywords

hair regeneration; motion-activated device; physical approach; rats and nude mice; growth factors

Alopecia, commonly known as hair loss, is classified as a dermatological disorder due to a growth factor deficiency and/or hair cycle disorder.[1–3] It is a common disease for both men and women throughout the world. In the United States, about 35 million men and 21 million women suffered from hair loss in 2015.[4] Currently, major treatments for hair loss include topical treatments, oral medicine, and hair transplant to re-establish healthy hair growth cycles.[5–7] Due to the non-invasive nature and high absorbability, topical treatments are the most common choice by patients. Minoxidil (MNX) and oral finasteride are the two drugs approved by the United States Food and Drug Administration and widely used to prevent and treat hair loss.[3,7] However, since MNX and finasteride could only reduce hair loss instead of significantly increasing the number of hair follicles (HFs), patients are thus required to continuously apply drugs for lasting effects.[8,9] Moreover, MNX and finasteride may induce severe side effects such as sexual dysfunction, hypertrichosis, and fetus defect.[5,7,10] As an alternative of taking medication, hair transplant may help patients grow new hair, but several rounds of surgery are needed, which are associated with high cost, discomfortness, and time commitment.[7] Therefore, non-invasive, nonpharmacological, cost-effective, and convenient approaches are always desired for treating hair loss. Currently, several promising nonpharmacological treatments such as thermal, laser, and electrical stimulation have been developed and are gradually moving into clinical investigation/practice.[8,11–13] Among them, electric stimulation can induce a non-invasive biological effect named electrotrichogenesis (ETG). Though the optimal ETG parameters have not been clinically confirmed, alternating electric field (EF) in the range of 0.1–10 V/cm and frequencies of <15 Hz are commonly used, which imposes negligible tissue damage.[14,15] ETG could enhance the influx of calcium ions into the dermal papilla cells *via* voltage-gated

transmembrane ion channels, facilitate ATP synthesis in mitochondria, activate protein kinases, and stimulate protein synthesis and cell division.[8,16,17] As a result, the ETG effect is believed to be able to regulate secretion of multiple hair growth factors, promote HF proliferation, prolong the anagen stage, and ultimately promote hair regeneration.[8,18,19] Although state-of-the-art extracorporeal treatment apparatuses have miniaturized their sizes to accommodate themselves to wearable devices, the entire system remains bulky and inconvenient for daily treatment as restricted by battery capacity and output current.[20–22]

Here, a universal motion-activated and wearable electric stimulation device (*m*-ESD) that can effectively promote hair regeneration *via* random body motions was designed. Significantly facilitated hair regeneration results were obtained from Sprague–Dawley (SD) rats and nude mice. Higher HF density and longer hair shaft length were observed on SD rats when the *m*-ESD was employed. We also showed that *m*-ESD can promote HFs proliferation and improve the secretion of vascular endothelial growth factor (VEGF) and keratinocyte growth factor (KGF) and thereby alleviate hair keratin disorder, increase the number of HFs, and promote hair regeneration on genetically defective nude mice. While rats and nude mice models were used in this study, human reconstructed skin in a mouse model will be a valuable next step to evaluating the human HFs generation effect under this kind of electric stimulation.[23,24]

RESULTS AND DISCUSSION

The *m*-ESD consists of two modules: an omnidirectional triboelectric generator (OTG) acting as the electric pulse generator and a pair of interdigitated dressing electrode providing spatially distributed EF (Figure 1a). The detailed fabrication process of the *m*-ESD is depicted in Figure S1. The structure details and key components of the OTG are illustrated in Figure 1b. The OTG had two triboelectric layers, which were connected by soft Ecoflex bands. The Ecoflex band had a very small modulus (34.9 kPa) (Figure S2a), which allowed arbitrary stretching, bending, and twisting within ~900% strain limit.[25,26] A pair of concentric gold (Au) electrode arrays on a nanostructured polytetrafluoroethylene (PTFE) film were designed as the charge transfer electrode (CTE) to collect the electrostatic charge generated during the movements. The CTE and interdigitated electrode were mounted on a polyethylene terephthalate (PET) substrate as the CTE layer. An array of concentric copper (Cu) ring electrodes was fabricated on a square PET acting as the bottom triboelectric layer for triboelectric charge generation (CGE). The entire OTG was encapsulated by polyimide films. The characterization results of the *m*-ESD cross section, the thickness of Au electrode, and the surface of the PTFE film are shown in Figure S2b–d. A typical *m*-ESD where the CTE and CGE layers were stretched apart from each other is shown in Figure 1c.

The mechanical behavior of the *m*-ESD was evaluated first. Three-dimensional finite element analysis (FEA) showed that when the *m*-ESD was stretched along the length directions, the strain was primarily distributed on the Ecoflex bands rather than on the PET substrates (Figure S3a). This ensures the stress subjected by the device can effectively induce the desired displacement of the OTG module. The uniaxial stretching behaviors were tested along length and width directions to generate electric pulses. The movements in the length and width directions generated nearly the same force–distance curves with a slope of

only 0.08 N/mm (Figure S3b), indicating excellent stretchability and symmetrical mechanical responses. Both computational and experimental measurements confirmed the OTG module can move freely along all different directions with minimal force requirements. In addition, the *m*-ESD was robust and could endure repeated twisting and stretching (Figure S4). This ensures a high potential for the application on irregular skin surfaces. In addition, cell viability test was conducted to confirm that the *m*-ESD encapsulated by polyimide film is noncytotoxic and biocompatible (Figure S5).

The electric pulses were controlled by designing the geometric parameters of CTE and CGE. As shown in Figure 1d, the ring width of CGE (d_G) was twice as that of CTE (d_T), while the ring number of CTE (n_G) was half of that of CGE (n_T). The working principle of the OTG is illustrated in Figure 1e. CTE contained two sets of electrodes and the open-circuit peak-to-peak voltages measured between them was defined as V_{PP}. Initially, when CGE slides against the triboelectrically negative PTFE layer, negative and positive charges are induced and evenly distributed on the PTFE and CGE surfaces, respectively.[27,28] Further placing the CGE under any set of CTE would lead to local charge unbalance. Under open circuit condition, the unbalance local charge would generate an electric potential difference between the two sets of CTE ($V_{PP} \neq 0$, stage i and (iii). As the CGE moved in between the two sets of CTE, the overall charge distribution is balanced and the electric potential reaches zero ($V_{PP} = 0$, stages ii and iv). Therefore, a periodic and cyclic alternating voltage output can be obtained while the two-layers of *m*-ESD stretched back and forth.

The CTE area was kept constant at 2×2 cm^2, and n_T was designed to be 4, 6, 10, and 12. Correspondingly, the outputs of four different CTE configurations ($d_T = 1.25$ mm, 830 μm, 500 μm, and 420 μm) (Figure S6) were investigated at a stretching velocity of 0.1 m/s for 1 cm displacement. As the CGE moved against CTE back and forth, electric pulse envelops were generated. Numbers of the electric pulse in each envelop were 2, 3, 5, and 6, respectively, consistent with the value of n_G (Figure 1f). When $n_T = 4$ and $d_T = 1.25$ mm, V_{PP} was ~340 mV. V_{PP} reached the maximum of 430 mV when $n_T = 6$ and $d_T = 830$ μm. V_{PP} then declined to 300 mV and 200 mV as d_T reduced to 500 and 420 μm, respectively. The reduction of V_{PP} could be attributed to the reduced surface area for charge collection. Considering the suitable V_{PP} and frequency, the OTG electrode with a d_G of 1 mm ($d_G = 2d_T = 1$ mm, $n_G = 5$, $n_T = 10$) and a V_{PP} of 300 mV was chosen for further animal studies. In addition, the pulse width of output was kept at 20 ms, which was within the reported pulse width range that could provide an effective stimulation with minimal side effects.[8,18,29–31]

The omnidirectional pulse generation capability of the *m*-ESD was then investigated under three different electrode traveling distances ($d = 0.5R$, $1.0R$, and $2.0R$, where R is the electrode radius). The relationships between the voltage, moving velocity, and directions were plotted for each d (Figure 2a). Similar plots were received for all three d, suggesting V_{PP} was not sensitive to the distance of traveling. The number of peaks in each voltage envelop increased from 3 to 5 to 10 as d increased from $0.5R$ to $1.0R$ to $2.0R$, respectively (Figure 2b). A strong relationship between V_{PP} and velocity can be clearly identified. For each d, V_{PP} increased monotonically from 80 mV to 720 mV, as the velocity raised from 0.05 to 0.4 m/s. This was consistent with other literature reports that higher velocity

facilitates efficient charge separation.[32–34] Most importantly, the equal-voltage lines in each plot exhibited a quasi-circular shape, confirming that V_{PP} was nearly the same when the *m*-ESD moves along all possible directions in plane. This result demonstrated that our *m*-ESD was able to produce stable voltage pulses in response to random lateral motions, which is perfect for interfacing with body movements.

The *m*-ESD was then applied to rats for hair regeneration studies. As schematically shown in Figure 2c, the *m*-ESD was attached to the backside of the rat. The CGE layer was affixed to the head of the rat, and the CTE layer was affixed to the neck and back area. Based on this setup, all random movements of the head and neck could generate electric pulses with similar amplitudes. These electric pulses were transmitted to the stationary dressing pad and provide alternating EFs to the exposed skin to stimulate hair regeneration. A SD rat wearing the *m*-ESD for hair regeneration test is shown in Figure 2d. The voltage output performance was monitored first when the rat was at its normal activity (Figure 2e and Movie S1). The voltage output from the rat's movements had a V_{PP} of 320 mV, similar to the voltage output induced by a computer-controlled shaker. This further confirmed that our *m*-ESD could effectively convert random body motions into stable electric pulses. The long-term stability of our *m*-ESD was tested by a commercial shaker. After 28 days of continuous operation, all the devices showed good structural integrity without any observable defects. The nearly unchanged voltage amplitude confirmed the excellent stability and durability of the *m*-ESD (Figure 2f and Movie S2). The highly flexible and stretchable device also induced minimal influences to the rat's normal daily behavior (Movie S3).

A typical hair growth begins inside the avascular HF and depends on the nutrition supplied by blood vessels (Figure 3a).[35] Hair undergoes periods of cyclic anagen (growth), catagen (regression), and telogen (resting) stages (Figure 3b).[36,37] It is known that the EF can act on the skin and promote HF proliferation and hair regeneration. Meanwhile, dermal papilla cells of HF are believed to be the most susceptible to the effects of electric stimulation in the skin.[17,18] In order to verify that the EF induced by our *m*-ESDs can promote HF transformation from the telogen stage to the anagen stage to achieve rapid hair regeneration, systematic experimental study of hair regeneration based on SD rats was conducted. First, the back hair of 7 week-old SD rats was shaved and treated with removal cream, which brought the hair follciles to the telogen stage.[38,39] To ensure the suitable distribution and intensity of EFs for systematic research, electrodes with different gaps (8 mm, 4 mm, 1 mm, and 0.5 mm) were employed to create an EF parallel to the shaved skin surface (Figure 3c). Considering that the V_{PP} is 300 mV at a velocity of 0.1 m/s, the corresponding peak-to-peak EF strengths were 0.375, 0.75, 3, and 6 V/cm, respectively. Both hair coverage (Figure 3d) and hair length (Figure 3e) measurements revealed that the 3 V/cm EF had the most significant hair regenerative effect. This optimal EF might be attributed to the mostly facilitated calcium influx under favorable EF strength, which provides better stimulations to cell proliferation, hair growth factor secretion, and hair regeneration.[13,14] FEA simulation (Figure 3f,g) showed that there was no significant attenuation for EF strength within 4 mm deep into the skin surface. This thickness of insulating polyimide film was 20 μm, which was almost 2 orders of magnitude less than the distance that the EF can effectively penetrate (4 mm). Therefore, the electric intensity applied on skin tissue was almost unchanged. As a control, rats wearing sham *m*-ESDs were monitored for 2 weeks, and no obvious signs of

hair regeneration were observed (Figure S7). We also showed that the hair regeneration exactly followed the EF distribution, as evidenced by a W-shaped hair pattern when a W-shaped electrode was used (Figure S7).

The hair regeneration efficacy of our *m*-ESD was further compared to conventional hair regeneration medicines including MNX, vitamin D_3 (VD_3), and normal saline (NS) ($n = 3$ for each group). The four different treatments were applied to four regions on the back of SD rats as shown in Figure 4a and Figure S8. After 3 weeks of treatment, hair in the *m*-ESD region was significantly longer and denser than the other three treated regions (Figure 4a, bottom). Hematoxylin and eosin (H&E) staining were conducted on the rat skin samples to reveal the hair regeneration behavior as a function of time (Figure 4b). According to the histomorphometric classification of different stages (Figure 3b), anagen HFs are morphologically distinct from those in the telogen stage. Compared to the control groups (MNX, VD_3, and NS), HFs under *m*-ESD transformed from the telogen stage to the anagen stage in the first week, while HFs in other groups maintained in the telogen stage. Heat map illustrates the regeneration trend of the hair shaft in the four regions. It is obvious that the *m*-ESD induced a much faster hair regeneration rate compared to the other three groups (Figure 4c). The average hair shaft length measured after 3 weeks of treatment revealed that the hair shaft at the *m*-ESD region was15.4 ± 2.1 mm, significantly longer than those in the control groups (8.7 ± 1.2 mm for MNX, 6.9 ± 0.9 mm for VD_3, and 3.4 ± 0.4 mm for NS, Figure 4d). HF proliferation percentage was calculated from the H&E lateral skin slices (Figure S9) at different time points to study the HF proliferation effect in different stimulation regions. According to others' previous work,[13,18,40] the HF proliferation in Figure 4e and Figure 5e was calculated according to the formula: $P_{HF} = (D_i - D_{NS})/D_{NS} \times 100\%$, where D_i represents the density of HF in the *m*-ESD, MNX, and VD_3 groups, respectively, while D_{NS} represents the density of HF in the NS group (Figures S9 and S14). As shown in Figure 4e, the HF density in the *m*-ESD region quickly rose to 76% in the first week and reached as high as 96% proliferation after 3 weeks; whereas, MNX and VD_3 induced a much slower proliferation rate and only reached 68% in the same 3-week frame. In addition, compared to the reported electrical stimulation and MNX approaches for clinical hair regeneration, our *m*-ESD demonstrated more rapid and generally more effective hair proliferation with a much shorter treatment time (Figure 4f).[16,18,19,41–43] This analysis confirmed that the self-generated electric pulses from *m*-ESD could significantly promote hair regeneration and HF proliferation in SD rats.

After confirming the positive effect on hair regeneration on SD rats, we further investigated how the electric pulses from *m*-ESD can influence the hair regeneration on genetically defective nude mice with a 21-day hair cycle.[40,44] The nude mice lack fur development due to deficiency of growth factors. On the skin of nude mice, the hair shafts bend and coil at the sebaceous gland and fail to penetrate the epidermis.[45,46] In order to match the body size, the *m*-ESD for nude mice was made smaller than that for the SD rats, while they had the same electrode configuration and geometry (Figure S10a). Since the V_{PP} was only related to the moving velocity, the nude mice could generate similar electric pulses as the rats' device under their regular movements (Figure S10b, Movies S4 and S5), and the *m*-ESD on nude mice exhibited a good stability (Figure S10c and Movie S6). The *m*-ESD-stimulated hair regeneration behavior was investigated during the 21-day growth period, in comparison to

the treatments of MNX, VD_3, and NS ($n = 4$ for each group). For the model of nude mice, the dorsal hair of nude mice was observed until completion of a hair growth cycle. The hairs disappearing was a result of hair growth entering the catagen and telogen phases.[40,44] Following catagen, follicles lie dormant in the telogen phase, and HF stem cells are activated at the telogen-to-anagen transition to initiate a new round of hair growth.[47] This phenomenon suggests that our electrical stimulation only facilitates hair growth but had minimal influences to the natural hair growth cycle. Longitudinal photos clearly showed that the *m*-ESD yielded significantly longer hair with higher density and longer appearing time than other control regions (Figure 5a and Figure S11). It should be noted that the location on the mice back had negligible impacts to the hair regeneration (Figure S12). The H&E staining of longitudinal slices of skin in different stimulated regions (*m*-ESD, MNX, VD_3 and NS) was conducted at different treatment time points (Figure 5b and Figure S13). After 3 days of treatment, the hair at the *m*-ESD-covered region transformed from the telogen stage to the anagen stage, while the hair in control regions still remained at the telogen stage. From day 6 to day 12, the hair at the *m*-ESD region still remained at the anagen stage; whereas the HFs started to shrink in the control regions (MNX, VD_3, and NS). As the hair in the *m*-ESD region gradually entered the catagen stage on the 15th day, the hair in control regions completed the anagen stage on day 12 and completely entered the telogen stage on day 15. These results showed that the *m*-ESD stimulations could effectively facilitate the transformation of HFs from the telogen stage to the anagen stage and extend the length of the anagen stage, that is, more fully developed hair with longer lifetime. A heat map of the hair shaft length for different treatments further quantified that faster and significantly longer hair growth was promoted by the *m*-ESD compared to other treatments (Figure 5c). After 9 days of treatment, the hair shaft under *m*-ESD was 1.81 ± 0.15 mm, nearly twice as long as those in the control groups (0.97 ± 0.17 mm and 0.93 ± 0.10 mm for MNX and VD_3, respectively) (Figure 5d). HF proliferation percentage of different groups over time (Figure 5e) was calculated from the H&E slices (Figure S14). The HF density of the *m*-ESD group showed a significant improvement after 12 days and topped at 33% at the 18th day of treatment. In contrast, the HF proliferation percentage in the MNX group and VD_3 group remained at nearly constant values of 11% and 7%, respectively. This analysis further confirmed that the *m*-ESD can enhance the HF cell proliferation, even overcoming the genetic defect (*e.g.*, hair keratin disorder) to develop visible hair on nude mice.

The accelerated hair regeneration and improved HF proliferation under the stimulation of *m*-ESD could be attributed to the EF regulation of growth factors secretion. To test this hypothesis, secretion of two main growth factors: keratinocyte growth factor (KGF), an important endogenous mediator of HF development and differentiation, and vascular endothelial growth factor (VEGF), a major mediator of HF growth and cycling, were studied.[34,40] Both factors together promote hair development and growth and increase HF numbers and hair size.[35,45] Many types of cells can secrete growth factors for cell proliferation and differentiation.[48–52] In this work, the follicular dermal papilla cells play the most crucial role in secreting growth factors and promoting hair regeneration.[35,45,53] KGF and VEGF expressions were investigated from the HFs at different treatment regions and imaged at various time points from day 3 to day 15 (Figure 6a,c). KGF is a member of the fibroblast growth factor (FGF) family that specifically induces proliferation of a wide variety

of epithelial cells, including keratinocytes within the epidermis and HFs.[45,46] In the developing HF, KGF is localized to HF and acts specifically on keratinocytes throughout the epithelial compartment of the HF. Thus, fluorescence intensity represents the concentration of the KGF, and the follicular epithelium (keratinocytes) has a stronger fluorescence intensity than that of follicular dermal papilla cells. Based on the fluorescence intensities, KGF and VEGF expression levels could be quantified (Figure 6b,d). As shown in Figure 6b, in the early anagen stage (day 3), no significant differences of KGF expression level were observed in different stimulation regions. At day 6, the KGF expression in the *m*-ESD region exhibited a sharp increase and reached the maximum at day 9, followed by a slight declination in the late anagen stage (day12) and early catagen stage (day 15). Nevertheless, it maintained the highest level throughout the entire testing period. For the control regions, the KGF expression remained at a significantly lower level during most of the study period. Though jumps of the KGF level were observed from the MNX and VD_3 treated regions (day 12 for MNX, day 6 for VD_3), the high expression levels cannot be maintained for a sustained period. As the only endogenous growth factor for normal development and differentiation of HFs, KGF could stimulate keratinocytes within HFs and sebaceous glands to eliminate genetic keratin disorder. Therefore, *m*-ESD was able to motivate the hair to penetrate the epidermis, promoting effective hair regeneration with visible dense hair on the skin of nude mice.

The VEGF expression exhibited a different trend during the testing period. As shown in Figure 6d, the VEGF expression in *m*-ESD region rapidly increased shortly after the stimulation. Up to day 6, its level was significantly higher than all the other control areas. Nevertheless, a constant decrease of VEFG expression in *m*-ESD region was observed after day 9, whereas MNX brought the VEFG level up to a similar level from the late anagen stage (day 12). When entering the catagen stage (day 15), all the *m*-ESD, MNX, and VD_3 regions exhibited a similar VEGF expression level, and the NS treated region had negligible VEGF remaining. The high VEGF level at the anagen stage is particularly important to enhance the perifollicular vascularization to meet the increased nutritional needs of HFs to achieve fast hair growth and increased HF density. These results confirmed that compared to conventional MNX and VD_3, simulations from our *m*-ESD can more effectively promote growth factor secretion and further prolong endogenous signaling to achieve accelerated hair regeneration.

CONCLUSION

In this work, we developed a self-powered omnidirectional *m*-ESD for accelerated hair regeneration on SD rats and nude mice. The *m*-ESD driven by irregular head motions generated consistent AC voltage pulses, which was directly used as a noninvasive EF to stimulate hair regeneration *via* a pair of interdigitated dressing electrodes. On shaved SD rats, the *m*-ESD was able to facilitate hair transformation from the telogen stage to the anagen stage and thereby accelerate hair growth rate and promote HF proliferation. Compared to the other conventional pharmacological MNX and VD_3 treatments, the hair growth rate in the *m*-ESD region was 0.73 mm per day (0.41 mm/day for MNX and 0.33 mm/day for VD_3), and the final hair shaft length under *m*-ESD was 1.8 times and 2.2 times

longer than those treated by MNS and VD_3, respectively. Meanwhile, the HF density from *m*-ESD stimulating was 141% of the MNX and VD_3 regions.

Importantly, the *m*-ESD stimulation could overcome the genetic keratin disorder and achieve effective hair regeneration on nude mice. This phenomenon can be attributed to a paracrine mechanism of hair growth factors (VEGF and KGF). KGF, as the only endogenous growth factor for HF development and differentiation, exhibited a higher expression level under *m*-ESD in the entire anagen stage, which can effectively normalize keratin differentiation to stimulate keratinocytes within HFs, eliminate genetic keratin disorder, and further develop visible hair with longer lifetime. VEGF showed a rapid increase from the beginning of the anagen stage, offering an advantage for induction of angiogenesis, and can enhance perifollicular vascularization to meet the increased nutritional needs of HFs for rapid cell division during anagen stage, leading to high hair growth rate and HF density. In addition, hair follicular stem cells (HFSCs) also play an important role in hair regeneration, such as reversing the pathological mechanism and regenerating HFs. To further understand the influences of the low-frequency alternating electrical fields on the HFSC activities, the HFSCs will provide valuable insights to this intriguing technology. In general, our development provided an effective hair regeneration strategy in the context of a nonpharmacological self-powered wearable electronic device. It is expected to be able to quickly evolve into a practical and facile solution to address the hair loss problem suffered by billions of people all over the world.

EXPERIMENTAL SECTION

m-ESD Fabrication.

PET (100 μm) and nanostructured PTFE substrates (50 μm) were prepared and sputtered with Au film (230 nm) to fabricate the interdigitated electrode and CTE, respectively. The CTE was installed on the PET substrate as the CTE layer, then the concentric Cu film (20 μm) was attached on a square PET substrate as the CGE layer. The two layers were assembled together and encapsulated with biocompatible polyimide film (20 μm). The top and bottom triboelectric layers were connected with Ecoflex bands $6 \times 3 \times 0.4$ ($L \times W \times T$) mm^3. A schematic flowchart of the specific fabrication process is shown in Figure S1. Due to the different body sizes of SD rats and nude mice, *m*-ESDs with different parameters match the body sizes. Device dimensions are 6×4 ($L \times W$) cm^2 for SD rats and 2.5×1.5 ($L \times W$) cm^2 for nude mice. In particular, the PTFE surface was treated by reactive ionic etching to introduce nanostructured features to enhance the electrical output. Specifically, 5 nm Au was sputtered on PTFE film first. Then the PTFE film was treated in an inductively coupled plasma chamber with mixed etching gases of Ar, O_2, and CF_4 for 30 s.[54,55]

Computational and Experimental Mechanical Properties of *m*-ESDs.

The computational mechanical properties were simulated by FEA, which ensures the reliability of the device (Figure S3a). For the experimental mechanical properties, using an Ecoflex strip with 30 mm original length and 0.4 mm thickness, which was stretched to 120 mm, the strain was calculated according to the formula $strain = \Delta L/L$ (Figure S2a). For the

m-ESDs, the top and the bottom layers were fixed and stretched along opposite directions. The *m*-ESD of SD rats was stretched by 1 cm (Figure S3b).

Cell Morphology and Immunofluorescence Staining.

After 3T3 cells were cultured on encapsulation or cell plates in 24-well plates, cell morphology was observed directly using an inverted optical microscope (Nikon Eclipse Ti–U, Japan). The cytoskeleton and nucleus were stained with Texas red-X phalloidin (591/608 nm) and blue fluorescent Hoechst (352/461 nm) (ThermoFisher Scientific), respectively. The samples were fixed with 2–4% formaldehyde for 15 min and then rinsed three times with prewarmed PBS. The samples were incubated with Texas red-X phalloidin (100 nM) and Hoechst (50 nM) for 30 min at 37 °C. After staining, cells were rinsed with prewarmed buffer for 3 times and imaged using a Nikon A1RS confocal microscope (Figure S5a).

MTT Assay.

After 3T3 cells were cultured on the packaging film on 24-well plates, a 3-{4,5-dimethylthiazol-2-thiazolyl}-2,5-diphenyl-2H-tetrazolium bromide (MTT) assay (ThermoFisher scientific) was performed to examine cell proliferation. After incubation at 37 °C in a humidified atmosphere with 5% CO_2 for up to 3 days, 100 μL of MTT solution was added to each well. After 4 h of incubation, the medium was removed, and DMSO (500 μL/well) was added to dissolve the precipitated fomazan. The optical density ($n = 3$) of the solution was evaluated using a microplate spectrophotometer at a wavelength of 490 nm (Figure S5b).

Electrical Output Performance Test and EF Simulation.

Open-circuit voltage was monitored when the *m*-ESD was stretched by commercial shaker and when the rat wearing the *m*-ESD was awakened. Open-circuit voltage was measured by a portable oscilloscope (Agilent, DSO1012A, internal resistance = 1 MΩ). The intensity and distribution of the EF in a real biological environment was simulated by ANSYS HFSS with an environmental dielectric constant of 80.

Animals and Diets.

All animal experiments were conducted under a protocol approved by the University of Wisconsin Institutional Animal Care and Use Committee. 7–8 week-old female Sprague–Dawley rats and nude mice were acquired from Envigo (New Jersey, USA). All animals were housed in separated cages in a temperature-controlled room (22 °C) with a 12 h light/dark cycle with free access to water and Purina PMI-certified rodent chow 5002 (LabDiet, MO, USA).

Hair Shaving and Removal.

A 15 cm^2 area of the hair from the dorsal portion of all the SD rats was shaved with electric hair clippers. Then the hair removal cream was evenly applied to the back. After 10 min, the back was cleaned with PBS solution.

Fixing Device on the Back of Animals (Rats and Mice).

In brief, anesthesia was induced by inhalation of 2–5% isoflurane and maintained with 2% isoflurane. Following anesthesia, animals were fixed in a prone position. The back of animals was scrubbed with iodine scrub and then alcohol prior to surgery. The device was placed on the back of the animals. The bottom layer of the *m*-ESD was sutured on the head skin of the animal, and the edge of the *m*-ESD was sutured on the back skin of the animal. For the *m*-ESD group, the two triboelectric layers were connected normally to the electrode. For the sham group, the device was sewed with insulated wires connecting to the electrode. The entire procedure lasted approximately 10 min.

Drug Application.

5% MNX solution was purchased from Kirkland Signature. The natural liquid VD_3 was purchased from Advanced Trichology. 0.2 mL was applied to the treatment area of the respective groups once a day, and a control group received no treatment. The hair regeneration of rats was monitored at days 7, 14, and 21, while for mice, hair regeneration was monitored at days 3, 6, 9, 12, 15, and 18 after the beginning of topical treatment. At each time point, rats and nude mice were sacrificed, and skin samples were collected for tissue sectioning and staining. Digital pictures of skin and hair were also taken, and hair samples were collected for qualitative and quantitative analysis.

Histological Staining of Skin Samples.

Skin samples were collected from the back of rats and nude mice after *m*-ESD, MNX, and VD_3 treatment. Control skin on the back was also collected with no treatment at the same time points. Tissues were embedded in Optimal Cutting Temperature compound (Sakura Fintek) and frozen overnight. Sectioning and H&E staining of all skin samples were performed by the University of Wisconsin-Madison Experimental Pathology laboratory. H&E slides were observed directly using an inverted optical microscope (Nikon Eclipse Ti–U, Japan).

For immunofluorescent staining, frozen skin samples of 10 μm thickness were fixed with cold acetone for 5 min, washed with cold PBS, and then blocked with 2% donkey serum for 1 h at room temperature. Slices were then incubated with rabbit-antirat/mouse VEGF antibody (Thermo Fisher) or rabbit-anti rat/mouse KGF antibody (Thermo Fisher) at 4 °C overnight. After washing with cold PBS for three times, slices were then stained with Alaxa488-labeled donkey-anti-rabbit antibody (Thermo Fisher) for 1 h. After three rounds of washing with cold Biotechnology and covered with cover slides for imaging using a Nikon A1R confocal microscope (Nikon instruments).

Quantitative Analysis of KGF and VEGF Expression Levels.

ImageJ software (version 1.52e) was used to quantify the expression levels of KGF and VEGF based on their fluorescent intensities, which were averaged over at least three different areas of a slide and expressed as mean ± standard deviation.

Statistical Analysis.

Statistical analysis was performed by two-tailed unpaired Student's *t* tests; n.s., nonsignificant ($P > 0.05$); *$P < 0.05$, **$P < 0.01$, ***$P < 0.001$. In box plots, the dot is the mean, center line is the median, box limits are the lower quartile (Q1) and upper quartile (Q3), and whiskers are the most extreme data points that are no more than 1.5 × (Q3 – Q1) from the box limits.

Supplementary Material

Refer to Web version on PubMed Central for supplementary material.

ACKNOWLEDGMENTS

This work was supported by the National Institute of Biomedical Imaging and Bioengineering of the National Institutes of Health under award number R01EB021336. W.C. thanks the support from the National Institutes of Health under award number P30CA014520. The content is solely the responsibility of the authors and does not necessarily represent the official views of the National Institutes of Health. G.Y. and Y.L. thank the National Basic Research Program of China (973 Program) under grant no. 2015CB351905.

REFERENCES

(1). Lei M; Chuong CM Aging, Alopecia, and Stem cells. Science 2016, 351, 559. [PubMed: 26912687]

(2). Matsumura H; Mohri Y; Binh NT; Morinaga H; Fukuda M; Ito M; Kurata S; Hoeijmakers J; Nishimura EK Hair Follicle Aging is Driven by Transepidermal Elimination of Stem Cells via COL17A1 Proteolysis. Science 2016, 351, aad4395. [PubMed: 26912707]

(3). Price VH Treatment of Hair Loss. N. Engl. J. Med 1999, 341, 964. [PubMed: 10498493]

(4). Marks DH; Penzi LR; Ibler E; Manatis-Lornell A; Hagigeorges D; Yasuda M; Drake LA; Senna MM The Medical and Psychosocial Associations of Alopecia: Recognizing Hair Loss as More Than a Cosmetic Concern. Am. J. Clin. Dermatol 2019, 20, 195–200. [PubMed: 30390206]

(5). Sasson M; Shupack JL; Stiller MJ Status of Medical Treatment for Androgenetic Alopecia. Int. J. Dermatol 1993, 32, 701–706. [PubMed: 8225706]

(6). Blumeyer A; Tosti A; Messenger A; Reygagne P; del Marmol V; Spuls PI; Trakatelli M; Finner A; Kiesewetter F; et al. Evidence-based (S3) Guideline for the Treatment of Androgenetic Alopecia in Women and in Men. J. Deutsch. Dermatol. Ges 2011, 9, S1–S57.

(7). Shapiro J Hair Loss in Women. N. Engl. J. Med 2007, 357, 1620–1630. [PubMed: 17942874]

(8). Benjamin B; Ziginskas D; Harman J; Meakin T Pulsed Electrostatic Fields (ETG) to Reduce Hair Loss in Women Undergoing Chemotherapy for Breast Carcinoma: A Pilot Study. Psycho-oncology 2002, 11, 244–248. [PubMed: 12112485]

(9). Banka N; Bunagan MJ; Shapiro J Pattern Hair Loss in Men: Diagnosis and Medical Treatment. Dermatol. Clin 2013, 31, 129. [PubMed: 23159182]

(10). Rogers NE; Avram MR Medical Treatments for Male and Female Pattern Hair Loss. J. Am. Acad. Dermatol 2008, 59, 547–566. [PubMed: 18793935]

(11). Asakawa M; Yoshioka T; Matsutani T; Hikita I; Suzuki M; Oshima I; Tsukahara K; Arimura A; Horikawa T; Hirasawa T; et al. Association of A Mutation in TRPV3 with Defective Hair Growth in Rodents. J. Invest. Dermatol 2006, 126, 2664–2672. [PubMed: 16858425]

(12). Lee HE; Lee SH; Jeong M; Shin JH; Ahn Y; Kim D; Oh SH; Yun SH; Lee KJ Trichogenic Photostimulation Using Monolithic Flexible Vertical AlGaInP Light-Emitting Diodes. ACS Nano 2018, 12, 9587–9595. [PubMed: 30125485]

(13). Sohn KM; Jeong KH; Kim JE; Park YM; Kang H Hair Growth-Promotion Effects of Different Alternating Current Parameter Settings Are Mediated by the Activation of Wnt/β-Catenin and MAPK Pathway. Exp. Dermatol 2015, 24, 958–963. [PubMed: 26268840]

(14). Mccullen SD; Mcquilling JP; Grossfeld RM; Lubischer JL; Clarke LI; Loboa EG Application of Low-frequency Alternating Current Electric Fields *via* Interdigitated Electrodes: Effects on Cellular Viability, Cytoplasmic Calcium, and Osteogenic Differentiation of Human Adipose-Derived Stem Cells. Tissue Eng., Part C 2010, 16, 1377–1386.

(15). Zheng Q; Zou Y; Zhang Y; Liu Z; Shi B; Wang X; Jin Y; Ouyang H; Li Z; Wang ZL Biodegradable Triboelectric Nanogenerator as a Life-Time Designed Implantable Power Source. Sci. Adv 2016, 2, No. e1501478. [PubMed: 26973876]

(16). Bureau JP; Ginouves P; Guilbaud J; Roux ME Essential Oils and Low-Intensity Electromagnetic Pulses in the Treatment of Androgen-Dependent Alopecia. Adv. Ther 2003, 20, 220–229. [PubMed: 14669818]

(17). Dąbrowski T. Hair Loss as a Consequence of Cancer Chemotherapy-Physical Methods of Prevention. A Review of the Literature. Wspolczesna Onkol 2011, 2, 95–101.

(18). Maddin WS; Bell PW; James JH The Biological Effects of a Pulsed Electrostatic Field with Specific Reference to Hair. Electrotrichogenesis. Int. J. Dermatol 1990, 29, 446–450. [PubMed: 2397975]

(19). Maddin WS; Amara I; Sollecito WA Electrotrichogenesis: Further Evidence of Efficacy and Safety on Extended Use. Int. J. Dermatol 1992, 31, 878–880. [PubMed: 1478771]

(20). Nan K; Kang SD; Li K; Yu KJ; et al. Compliant and Stretchable Thermoelectric Coils for Energy Harvesting in Miniature Flexible Devices. Sci. Adv 2018, 4, No. eaau5849. [PubMed: 30406207]

(21). Park S; Heo SW; Lee W; Inoue D; Jiang Z; Yu K; Jinno H; Hashizume D; Sekino M; Yokota T; Fukuda K; Tajima K; Someya T Self-Powered Ultra-Flexible Electronics *via* Nano-Grating-Patterned Organic Photovoltaics. Nature 2018, 561, 516–521. [PubMed: 30258137]

(22). Pinna M Device for Retarding Hair Loss and for Stimulating Its Regrowth U.S. Patent 5,595,564A, 1997.

(23). Wu X; Scott L; Washenik K; Stenn K Full-Thickness Skin with Mature Hair Follicles Generated from Tissue Culture Expanded Human Cells. Tissue Eng., Part A 2014, 20, 3314–3321. [PubMed: 25074625]

(24). Mi J; Chen S; Xu L; Wen J; Xu X; Wu X Human Reconstructed Skin in a Mouse Model In Skin Tissue Engineering: Methods and Protocols; Böttcher-Haberzeth S, Biedermann T, Eds.; Springer: New York, 2019; pp 227–237.

(25). Muth JT; Vogt DM; Truby RL; Menguc Y; Kolesky DB; Wood RJ; Lewis JA Embedded 3D Printing of Strain Sensors within Highly Stretchable Elastomers. Adv. Mater 2014, 26, 6307–6312. [PubMed: 24934143]

(26). Xu S; Zhang Y; Cho J; Lee J Stretchable Batteries with Self-similar Serpentine Interconnects and Integrated Wireless Recharging Systems. Nat. Commun 2013, 4, 1543. [PubMed: 23443571]

(27). Li A; Zi Y; Guo H; Zhong LW; Fernández FM Triboelectric Nanogenerators for Sensitive Nano-Coulomb Molecular Mass Spectrometry. Nat. Nanotechnol 2017, 12, 481–487. [PubMed: 28250471]

(28). Cheng J; Ding W; Zi Y; Lu Y; Ji L; Liu F; Wu C; Wang ZL Triboelectric Microplasma Powered by Mechanical Stimuli. Nat. Commun 2018, 9, 3733. [PubMed: 30213932]

(29). Golberg A; Khan S; Belov V; Quinn KP; Albadawi H; Felix Broelsch G; Watkins MT; Georgakoudi I; Papisov M; Mihm MC Jr.; et al. Skin Rejuvenation with Non-Invasive Pulsed Electric Fields. Sci. Rep 2015, 5, 10187. [PubMed: 25965851]

(30). Golberg A; Broelsch GF; Bohr S; Mihm MC; Austen WG; Albadawi H; Watkins MT; Yarmush ML Non-thermal, Pulsed Electric Field Cell Ablation: A Novel Tool for Regenerative Medicine and Scarless Skin Regeneration. Technology 2013, 01, 1–7.

(31). Khan S; Golberg A; McCormack M; Bei M; Yarmush M; Austen WG Hair Stimulation with Pulsed Electric Fields. Plast. Reconstr. Surg 2015, 136, 30.

(32). Shang W; Gu GQ; Yang F; Zhao L; Cheng G; Du Z.-l.; Wang ZL A Sliding-Mode Triboelectric Nanogenerator with Chemical Group Grated Structure by Shadow Mask Reactive Ion Etching. ACS Nano 2017, 11, 8796–8803. [PubMed: 28832113]

(33). Pu X; Guo H; Chen J; Wang X; Xi Y; Hu C; Wang ZL Eye Motion Triggered Self-Powered Mechnosensational Communication System Using Triboelectric Nanogenerator. Sci. Adv 2017, 3, No. e1700694. [PubMed: 28782029]

(34). Xie Y; Wang S; Niu S; Lin L; Jing Q; Yang J; Wu Z; Wang ZL Grating-Structured Freestanding Triboelectric-Layer Nanogenerator for Harvesting Mechanical Energy at 85% Total Conversion Efficiency. Adv. Mater 2014, 26, 6599–6607. [PubMed: 25156128]

(35). Yano K; Brown LF; Detmar M Control of Hair Growth and Follicle Size by VEGF-Mediated Angiogenesis. J. Clin. Invest 2001, 107, 409–417. [PubMed: 11181640]

(36). Fuchs E Scratching the Surface of Skin Development. Nature 2007, 445, 834. [PubMed: 17314969]

(37). Plikus MV; Mayer JA; de la Cruz D; Baker RE; Maini PK; Maxson R; Chuong C-M Cyclic Dermal BMP Signalling Regulates Stem Cell Activation During Hair Regeneration. Nature 2008, 451, 340. [PubMed: 18202659]

(38). Harel S; Higgins CA; Cerise JE; Dai Z; Chen JC; Clynes R; Christiano AM Pharmacologic Inhibition of JAK-STAT Signaling Promotes Hair Growth. Sci. Adv 2015, 1, No. e1500973. [PubMed: 26601320]

(39). Smith AA; Li J; Liu B; Hunter D; Pyles M; Gillette M; Dhamdhere GR; Abo A; Oro A; Helms JA Activating Hair Follicle Stem Cells *via* R-spondin2 to Stimulate Hair Growth. J. Invest. Dermatol 2016, 136, 1549–1558. [PubMed: 27109869]

(40). Begum S; Gu L-J; Lee M-R; Li Z; Li J-J; Hossain MJ; Wang Y-B; Sung CK *In Vivo* Hair Growth-Stimulating Effect of Medicinal Plant Extract on BALB/c Nude Mice. Pharm. Biol 2015, 53, 1098–1103. [PubMed: 25612775]

(41). Landau M; Lotti T; Yutskovskaya Y Efficacy Evaluation of a Novel Homeused Device Based on a Multiple Stimulation Technology on Hair Growth in Patients with Androgenetic Alopecia. Madridge J. Dermatol. Res 2018, 3, 70.

(42). Verner I; Lotti T Clinical Evaluation of a Novel Fractional Radiofrequency Device for Hair Growth: Fractional Radiofrequency for Hair Growth Stimulation. Dermatol. Ther 2018, 31, No. e12590. [PubMed: 29334164]

(43). Price VH; Menefee E; Strauss PC Changes in Hair Weight and Hair Count in Men with Androgenetic Alopecia, after Application of 5% and 2% Topical Minoxidil, Placebo, or no Treatment. J. Am. Acad. Dermatol 1999, 41, 717–721. [PubMed: 10534633]

(44). Müller-Röver S; Foitzik K; Paus R; Handjiski B; van der Veen C; Eichmüller S; Mckay IA; Stenn KS A Comprehensive Guide for the Accurate Classification of Murine Hair Follicles in Distinct Hair Cycle Stages. J. Invest. Dermatol 2001, 117, 3–15. [PubMed: 11442744]

(45). Danilenko DM; Ring BD; Yanagihara D; Benson W; Wiemann B; Starnes CO; Pierce GF Keratinocyte Growth Factor Is an Important Endogenous Mediator of Hair Follicle Growth, Development, and Differentiation. Normalization of the Nu/nu Follicular Differentiation Defect and Amelioration of Chemotherapy-Induced Alopecia. Am. J. Pathol 1995, 147, 145–154. [PubMed: 7604876]

(46). Mecklenburg L; Tychsen B; Paus R Learning from Nudity: Lessons From the Nude Phenotype. Exp. Dermatol 2005, 14, 797–810. [PubMed: 16232301]

(47). Alonso L; Fuchs E The Hair Cycle. J. Cell Sci 2006, 119, 391–393. [PubMed: 16443746]

(48). Botchkarev VA; Kishimoto J Molecular Control of Epithelial–Mesenchymal Interactions During Hair Follicle Cycling.J. Invest. Dermatol. Symp. Proc 2003, 8, 46–55.

(49). Yang JA; Chung H-M; Won C-H; Sung J-H Potential Application of Adipose-Derived Stem Cells and Their Secretory Factors to Skin: Discussion from Both Clinical and Industrial Viewpoints. Expert Opin. Biol. Ther 2010, 10, 495–503. [PubMed: 20218919]

(50). Chong HW; Park GH; Wu X; Tran TN; Park K; Park BS; Dong YK; Kwon O; Kim KH The Basic Mechanism of Hair Growth Stimulation by Adipose-Derived Stem Cells and Their Secretory Factors. Curr. Stem Cell Res. Ther 2017, 12, 535. [PubMed: 28875863]

(51). Ramdasi S; Tiwari SK Human Mesenchymal Stem Cell-Derived Conditioned Media for Hair Regeneration Applications. J. Stem. Cells 2016, 11, 201–211. [PubMed: 28296872]

(52). Kanji S; Das H Advances of Stem Cell Therapeutics in Cutaneous Wound Healing and Regeneration. Mediators Inflammation 2017, 2017, 1–14.

(53). Goodman LV; Ledbetter SR Secretion of Stromelysin by Cultured Dermal Papilla Cells: Differential Regulation by Growth Factors and Functional Role in Mitogen-Induced Cell Proliferation. J. Cell. Physiol 1992, 151, 41–49. [PubMed: 1560047]

(54). Yao G; Kang L; Li J; Long Y; Wei H; Ferreira CA; Jeffery JJ; Lin Y; Cai W; Wang X Effective Weight Control via an Implanted Self-Powered Vagus Nerve Stimulation Device. Nat. Commun 2018, 9, 5349. [PubMed: 30559435]

(55). Zhu G; Pan C; Guo W; Chen CY; Zhou Y; Yu R; Wang ZL Triboelectric-Generator-Driven Pulse Electrodeposition for Micropatterning. Nano Lett 2012, 12, 4960. [PubMed: 22889363]

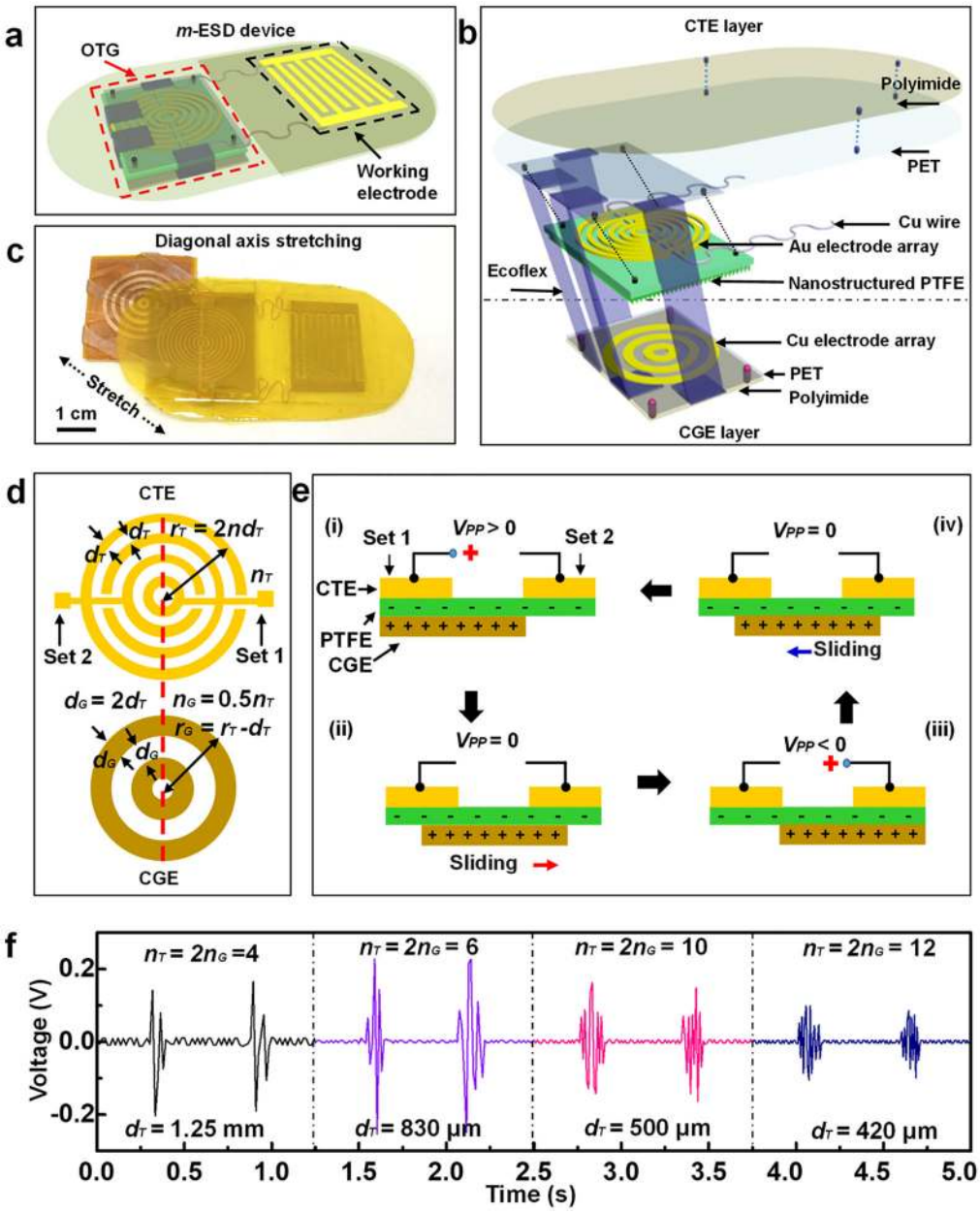

Figure 1.

Design and working principle of the motion-activated electric stimulation device (*m*-ESD). (a) Schematic configuration of the *m*-ESD consisting of an OTG and interdigitated dressing electrodes. (b) Enlarged-view scheme of the key components of the OTG including the CTE layer and CGE layer. (c) Optical image of the *m*-ESD stretched to show two functional layers of the OTG. (d) Geometric parameters of the gold CTE and copper CGE. The red dotted line is the central axis along the length direction. (e) Working principle of the OTG by sliding reversibly along any direction; (i) to (iv) represent different stages of charge transfer. (f) Representative voltage outputs of the OTG with different geometric parameters.

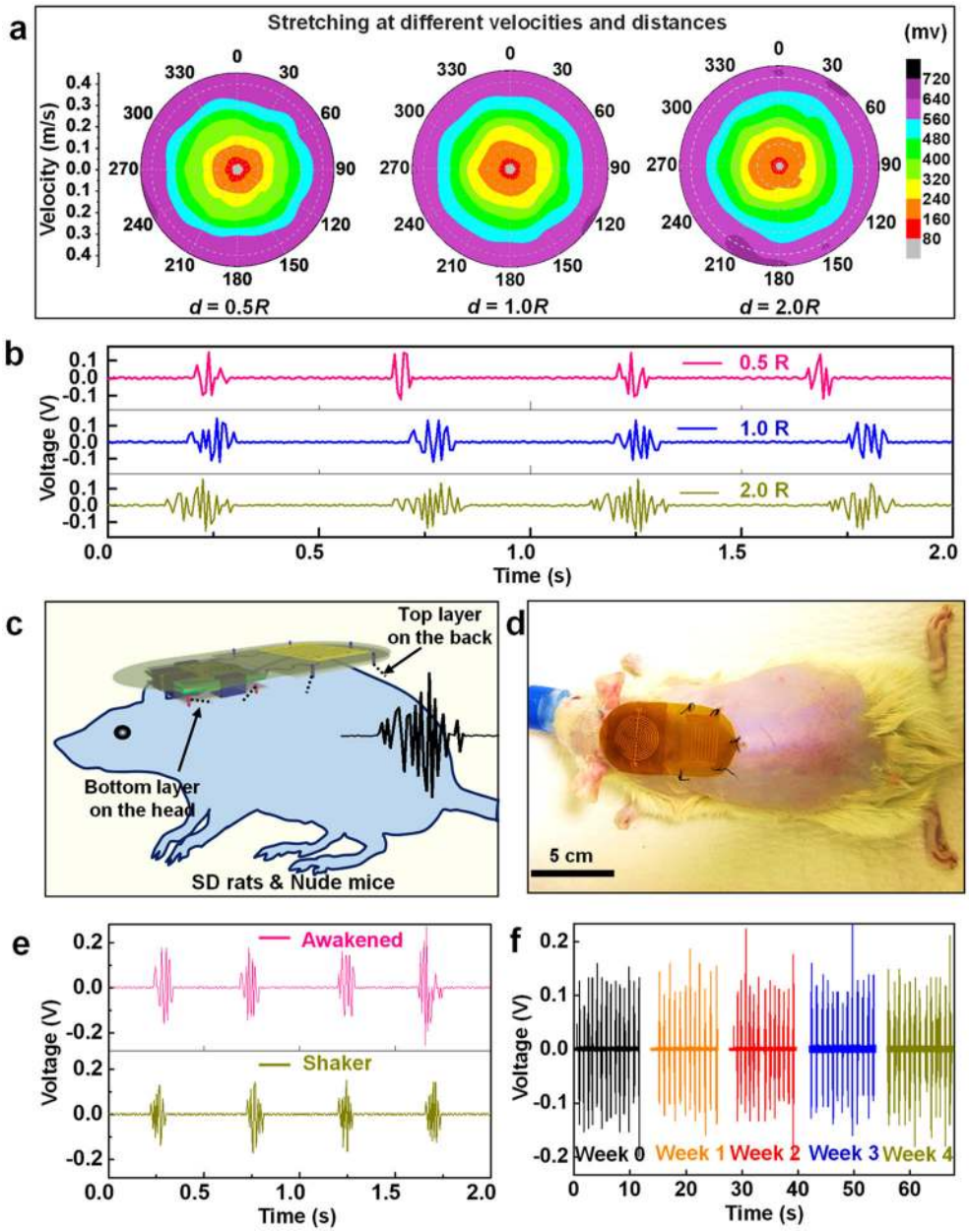

Figure 2.

Voltage output performance of the omnidirectional *m*-ESD. (a) Voltage output of the m-ESD stretching at different directions, velocities, and distances (*d* is the displacement distance and *R* represents the electrode radius). (b) Voltage peaks with regard to different displacement distances. (c) Schematic setup of the *m*-ESD system for hair regeneration. (d) Optical image of a SD rat wearing the *m*-ESD. (e) Voltage output recorded from the *m*-ESD on an active rat (awakened) and driven by a commercial shaker, respectively. (f) Stability and durability tests of the *m*-ESD.

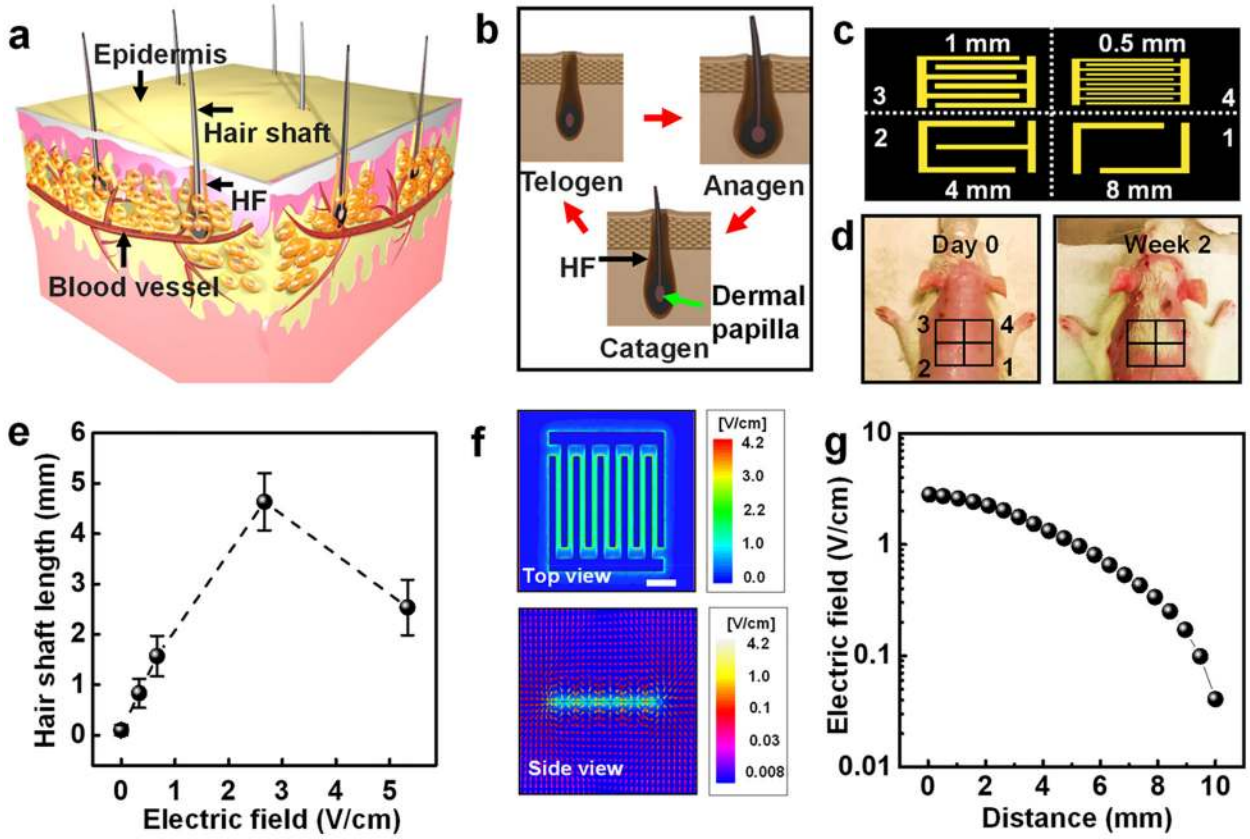

Figure 3.

Hair regeneration effect of SD rats under the stimulation of the *m*-ESD. (a) Schematic illustration of HFs in skin. (b) Histomorphology schematic of the hair cycle including anagen, catagen, and telogen stages. (c) Schematic diagram of a series of interdigitated electrodes (1–4) with different gap widths. (d) Optical images of the rat with removed hair (day 0, left) and after 2-week treatment (right). (e) EF-stimulated hair shaft length as a function of the EF intensity ($n = 6$). (f) Top and side views of EF distribution (gap width is 1 mm) simulated by ±150 mV. (g) EF strength at different distances perpendicular to the plane of the interdigitated electrode (gap = 1 mm). All data in (e) are presented as mean ± s.d.

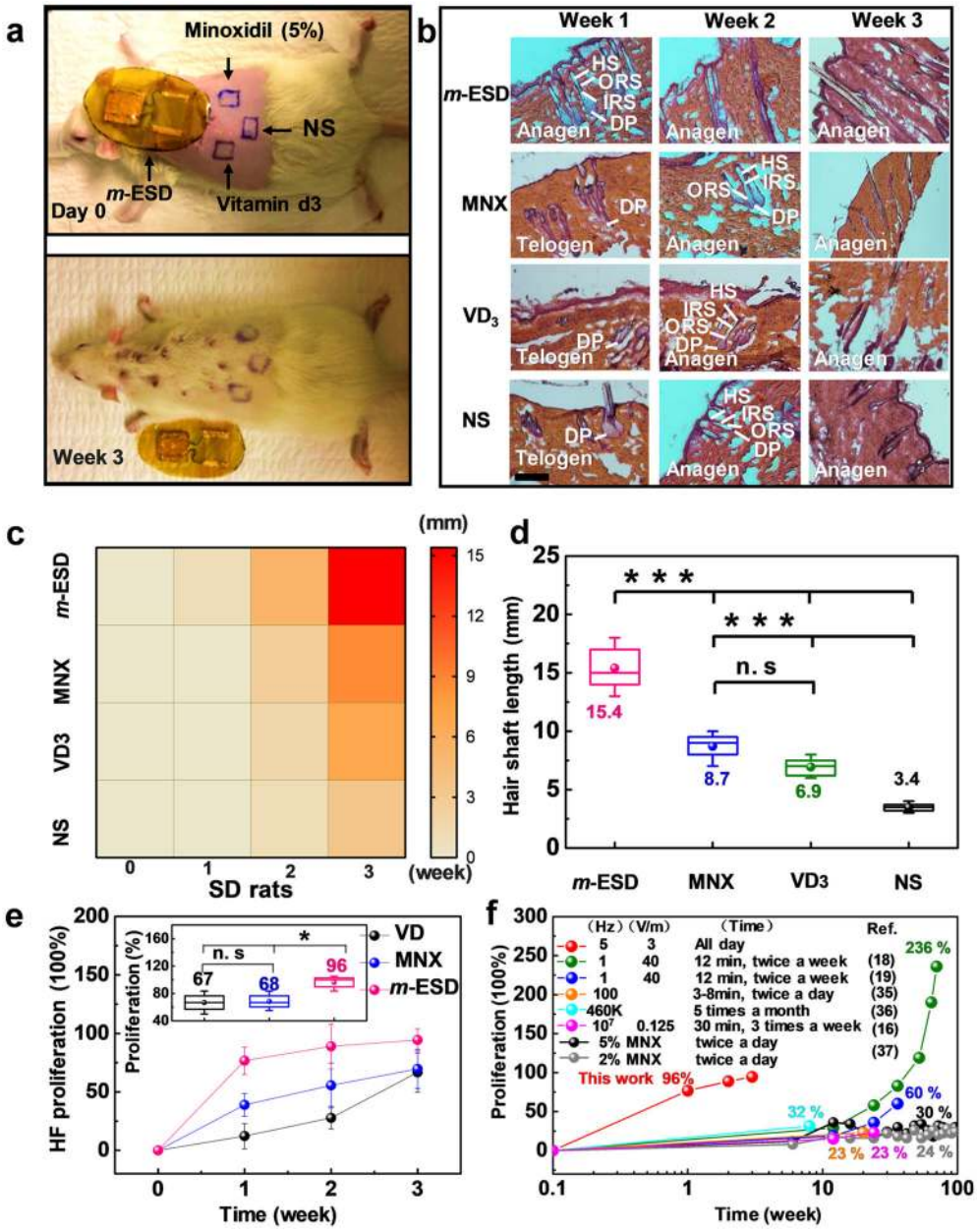

Figure 4.

Hair regeneration effect of SD rats under different treatment methods. (a) Comparison of hair regeneration under the influence of *m*-ESD, Minoxidil (MNX), vitamin D_3 (VD_3), and normal saline (NS); top: as-shaved rat; bottom: after 3-week treatment. (b) H&E staining of the epidermis under different treatment methods and time (scale bar = 200 μm). (c) Heat map of the hair shaft length from the four different treatment methods (*m*-ESD, MNX, VD_3, and NS) as a function of time. (d) Final hair shaft length of rats in the four experimental groups ($n = 6$). (e) HF proliferation of different groups over time ($n = 3$ for each group). The inset shows the HF proliferation percentage at the third week. (f) Hair proliferation percentage as a functional of treatment time (red dots) in comparison to the reported results by electric stimulation with different treatment parameters and MNX. All data in (e) are

presented as mean ± s.d. In (d) and the inset of (e) (box plots), dots are the mean, center lines are the median, box limits are the lower quartile (Q1) and upper quartile (Q3), and whiskers are the most extreme data points that are no more than 1.5 × (Q3 – Q1) from the box limits. Statistical analysis was performed by two-tailed unpaired Student's *t* tests; n.s., nonsignificant ($P > 0.05$); *$P < 0.05$, **$P < 0.01$, ***$P < 0.001$.

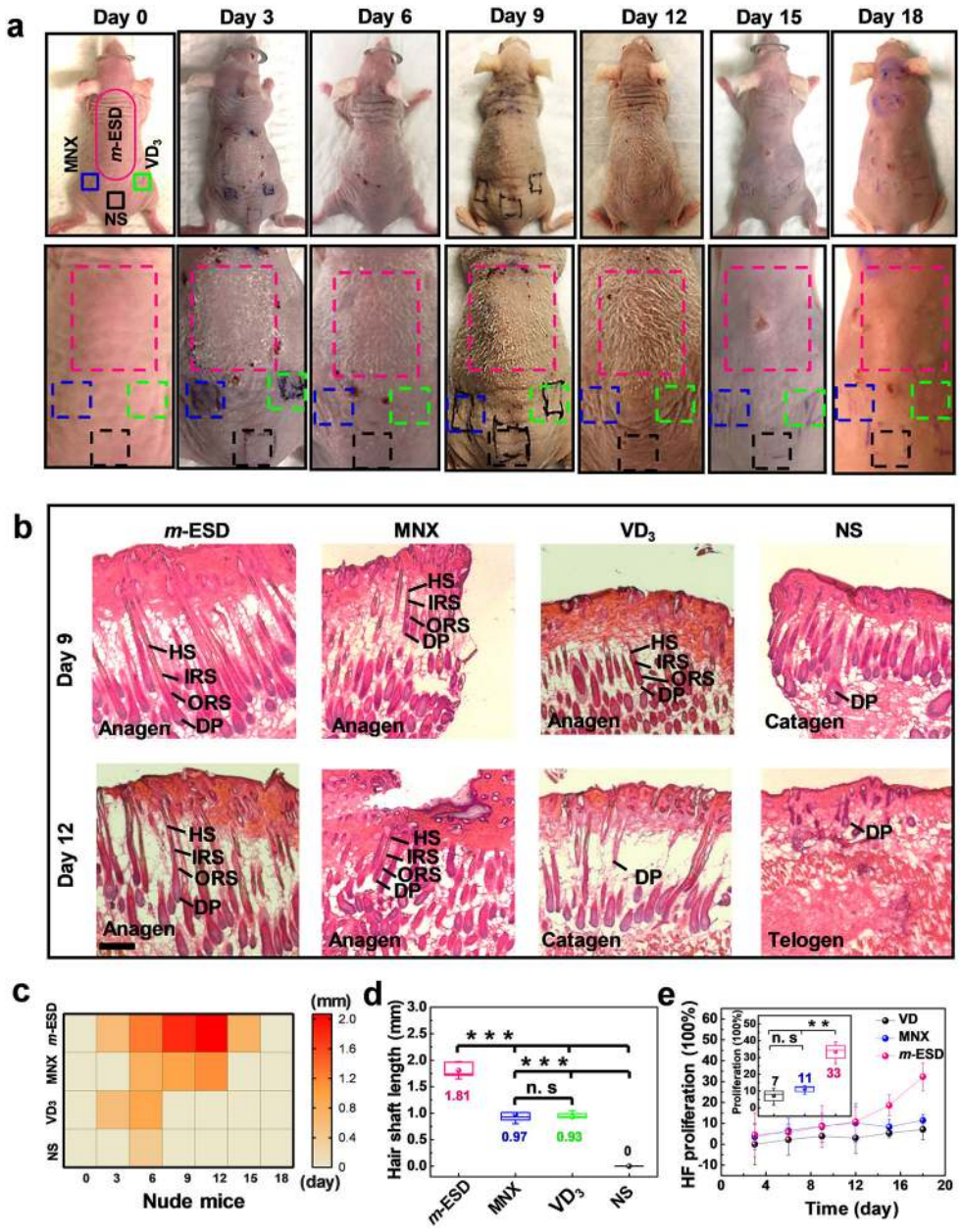

Figure 5.

Hair regeneration effect of nude mice under stimulation of *m*-ESDs. (a) Optical images of nude mice at different treatment times. (b) H&E staining of longitudinal slices of the epidermis under different stimulation time (scale bar = 200 μm). (c) Heat map of the hair shaft length as a function of time under the treatment regions of *m*-ESD, MNX, VD_3, and NS. (d) Final hair shaft length of nude mice in different treatment groups ($n = 6$). (e) HF proliferation percentage of different treatment groups as a function of time ($n = 3$). Inset shows the HF proliferation percentage at the 18th day. All data in (e) are presented as mean ± s.d. In (d) and the inset of (e) (box plots), dots are the mean, center lines are the median, box limits are the lower quartile (Q1) and upper quartile (Q3), and whiskers are the most extreme data points that are no more than 1.5 × (Q3 – Q1) from the box limits. Statistical

analysis was performed by two-tailed unpaired Student's *t* tests; n.s., nonsignificant ($P > 0.05$); *$P < 0.05$, **$P < 0.01$, ***$P < 0.001$.

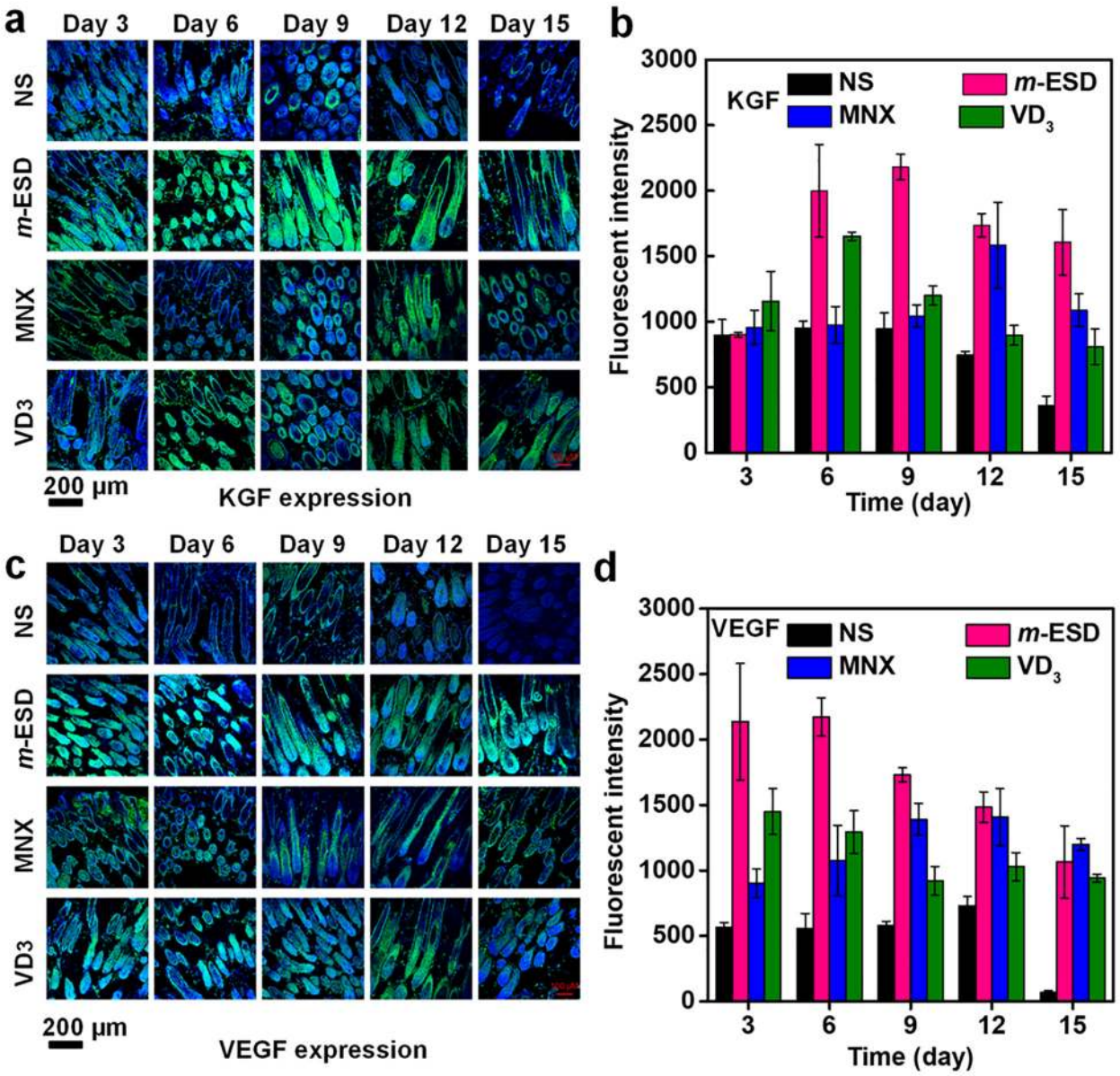

Figure 6.

Growth factor expression in skin of nude mice under stimulation of *m*-ESDs. (a) Confocal imaging of the KGF expression as a function of time for different treatments. (b) Fluorescence intensity of KGF quantitative expression ($n = 3$). (c) Confocal imaging of the VEGF expression as a function of time for different treatments. (d) Fluorescence intensity of VEGF quantitative expression ($n = 3$). All data in (b) and (d) are presented as mean ± s.d.